ADVANCED FUNCTIONAL MATERIALS
www.afm-journal.de

Single-Material OECT-Based Flexible Complementary Circuits Featuring Polyaniline in Both Conducting Channels

Lorenzo Travaglini, Adam P. Micolich, Claudio Cazorla, Erica Zeglio, Antonio Lauto, and Damia Mawad**

The organic electrochemical transistor (OECT) with a conjugated polymer as the active material is the elementary unit of organic bioelectronic devices. Improved functionalities, such as low power consumption, can be achieved by building complementary circuits featuring two or more OECTs. Complementary circuits commonly combine both *p*- and *n*-type transistors to reduce power draw. While *p*-type OECTs are readily available, *n*-type OECTs are less common mainly due to poor stability of the *n*-type active channel material in aqueous electrolyte. Here, a complementary circuit is made using a pair of OECTs having polyaniline (PANI) as the channel material in both transistors. PANI, with a finite electrochemical window accessible at voltages lower than 1 V, exhibits a peak in current versus gate voltage when used as an active channel in an OECT. The current peak has two slopes, one *n*-like and one *p*-like, which correspond to different electrochemical regimes of the same underlying conjugated polymer. The electrochemistry enables the design of a complementary circuit using only PANI as the channel material. The PANI-based circuit is shown to have excellent performance with gain of ≈7 and is transferred on a flexible biocompatible chitosan substrate with demonstrated operation in aqueous electrolyte.

1. Introduction

Organic and flexible bioelectronic devices are envisioned to impact future medical applications[1] in clinical diagnostics and therapeutics.[2–4] The organic electrochemical transistor (OECT) is the elementary unit of these devices, with advanced functionality including high signal-to-noise ratio recording or signal amplification.[5,6] Further applications are achieved by building integrated circuits that feature more than one OECT. The simplest example is a complementary logic circuit, which normally features *p*-type (hole majority) and *n*-type (electron majority) transistors to reduce power draw (**Figure 1**A). The operating gate input range is chosen such that when one transistor is "on" the other is "off," and vice versa. This makes the output swing between the drive voltage V_{DD} (*p*-transistor on/*n*-transistor off–*p*-slope in Figure 1A) and ground (*p*-transistor off/*n*-transistor on–*n*-slope in Figure 1A). The advantage to the complementary architecture is that power draw is reduced by having one of the two devices always in its off state. Complementary circuits are thus widely used in electronics applications with demanding energy supply/dissipation requirements. Both requirements are relevant to bioelectronics, where circuits can require long operation on limited battery supply, e.g., implants, and minimal heat dissipation to prevent tissue/cell damage and device degradation.[7] The complementary circuit described above uses a pair of unipolar transistor devices.[8–10] A more exotic alternative involves a pair of identical ambipolar transistor devices,[10] where both carrier types can be accessed within the available gate voltage V_{GS} range. Note that such transistors can either be an interpenetrating

Dr. L. Travaglini, Dr. C. Cazorla, Dr. E. Zeglio, Dr. D. Mawad
School of Materials Science and Engineering
UNSW Sydney
Sydney, New South Wales 2052, Australia
E-mail: damia.mawad@unsw.edu.au
Dr. L. Travaglini, Dr. E. Zeglio, Dr. D. Mawad
Centre for Advanced Macromolecular Design
UNSW Sydney
Sydney, New South Wales 2052, Australia
Prof. A. P. Micolich
School of Physics
UNSW Sydney
Sydney, New South Wales 2052, Australia
E-mail: adam.micolich@nanoelectronics.physics.unsw.edu.au
The ORCID identification number(s) for the author(s) of this article can be found under https://doi.org/10.1002/adfm.202007205.
Dr. E. Zeglio
Division of Micro and Nanosystems
KTH Royal Institute of Technology
Stockholm 10044, Sweden
Prof. A. Lauto
School of Science
Western Sydney University
Locked Bag 1797, Penrith, NSW 2751, Australia
Dr. D. Mawad
Australian Centre for Nano Medicine and ARC Centre of Excellence in Convergent Bio-Nano Science and Technology
UNSW Sydney
Sydney, New South Wales 2052, Australia

DOI: 10.1002/adfm.202007205

© 2020 Wiley-VCH GmbH

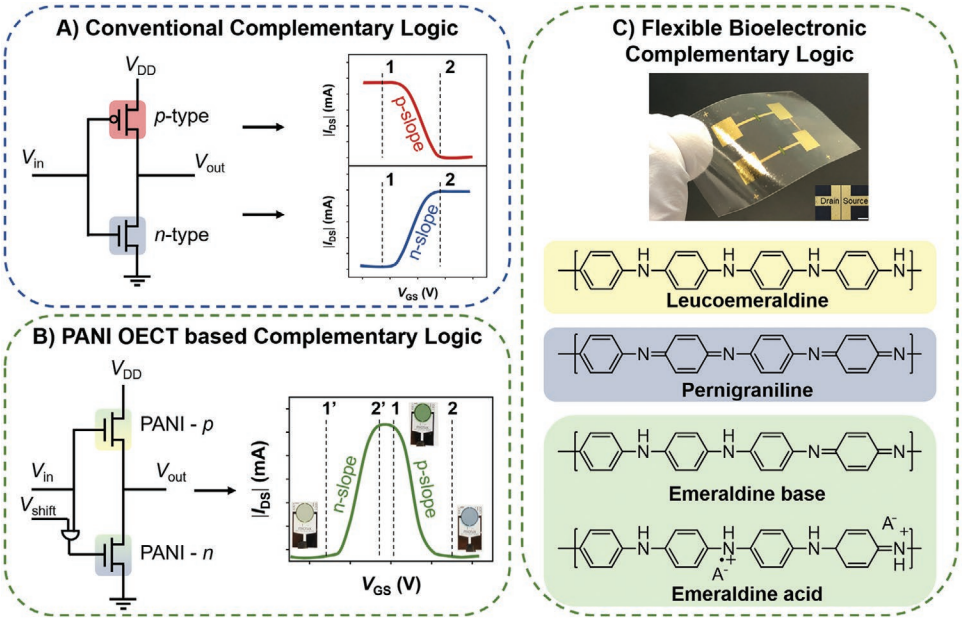

Figure 1. A) Schematic presentation of a conventional unipolar complementary logic circuit. B) Schematic presentation of our PANI OECT based complementary logic circuit. C) Digital image of the complementary logic circuit built on a flexible chitosan substrate (top), and chemical structures of PANI in its different oxidation states (bottom). The inset is an optical micrograph of the gold contacts of an individual transistor (scale bar 500 µm).

blend of organic *n*-like and *p*-like semiconductors[11] or a single material with some span of insulating behavior between the *p*-like and *n*-like conduction regions.[12,13]

Circuit designs featuring both unipolar and ambipolar transistors can pose serious challenges for conjugated polymer semiconductors. Conjugated polymers are predominantly *p*-type materials; the *n*-type polymeric semiconductors synthesized to date have relatively lower carrier mobility than *p*-type,[14,15] largely due to intrinsic conformational distortion in the polymer backbone.[16] This mobility mismatch has a detrimental effect on circuit performance. An additional consideration for bioelectronics is the need for the *n*-type polymer to have an operational electrochemical window compatible with aqueous electrolyte.[15] This further limits the availability of *n*-type materials, with only two reported to date.[14,15] Indeed, only one OECT-based complementary circuit using *n*-type and *p*-type conjugated polymers has been reported so far.[14] A design featuring ambipolar devices also requires well matched charge transport properties in the *p*- and *n*-type operating regimes.[11] This again limits material choice because in many ambipolar materials the electron and hole transport mobilities differ due to charge-disorder effects.[10] Furthermore, current synthetic techniques are complex and purification of the polymer is very challenging with trace metals occasionally detected in the product.[17,18] Thus, a major quest in the field of bioelectronics has been to find high performing *n*-type or ambipolar OECT materials with well-matched charge transport, ideally with streamlined synthesis and favorable device processing properties, to further develop OECT-based circuits for applications in neural sensing,[19] ion-logic and "iontronics,"[20] and biosymbiotic systems, e.g., electronic plants.[21] Here, we demonstrate the design of electrochemically driven OECT-based complementary circuits made using a pair of transistors containing the same channel material (Figure 1B). As the channel material, we use the well-established conjugated polymer polyaniline (PANI), one of the first organic semiconductors tested in transistors.[22] Our complementary circuit design exploits a known but previously unutilized feature of PANI discovered by Paul et al.[22] in 1985. PANI gave a peak in current versus V_{GS} when used as an OECT channel, in stark contrast to the monotonic increase/decrease obtained for a conventional unipolar transistor channel.[10] This conductivity peak provides a path to obtaining both *p*-like and *n*-like behavior in the same transistor channel (see Figure 1B). Circuits designed to cleverly exploit this conductivity peak were not explored at the time; we address this gap here.

Our complementary circuit consists of two identical PANI OECTs connected in series between a V_{DD} and ground, as usual. The PANI OECT closest to V_{DD} is operated on the *p*-slope side of the conductance peak (between 1 and 2 in Figure 1B) by directly applying the input voltage V_{in} to its gate electrode. The PANI OECT closest to ground is operated on the *n*-slope side (between 1' and 2' in Figure 1B) by shifting the input voltage supplied to its gate electrode by a dc offset $V_{shift} = -0.4$ V. This arrangement is chosen such that one PANI transistor is "on" while the other is "off" enabling complementary circuit operation. We determined an appropriate value for V_{shift} from the transfer characteristics, as discussed later. A crucial point to note is that polyaniline is not a traditional ambipolar material in our mode of operation–conduction is via hole majority transport across the entire operating range,[23,24] and the *p*-like and *n*-like slopes are on opposite sides of a conductivity peak rather than a conductivity valley (i.e., polyaniline = *n*-peak-*p*, traditional ambipolar = *p*-valley-*n*). The peak's symmetry means that the two OECTs in our circuit, operated on opposite sides of the peak, have intrinsically matched characteristics that afford strong potential for complementary

© 2020 Wiley-VCH GmbH

circuit use. Using a pair of identical PANI OECTs eliminates the need to develop a second material with matching performance for the small cost of adding a voltage shift apparatus into our input circuit, thereby overcoming a major roadblock to making OECT-based circuits. We also demonstrate that the technology can be transferred onto a flexible biocompatible chitosan substrate[25–29] operating in an aqueous electrolyte (Figure 1C), thus paving the way towards the realization of electrochemically driven complementary logic circuits based on two identical OECTs for potential applications in organic bioelectronics.

2. Results

2.1. Characterization of PANI-Based OECTs

For initial studies, PANI OECTs were fabricated on interdigitated gold microelectrodes (IDME) patterned on a glass substrate (PANI-on-IDME OECT). The IDME's serpentine structure gives a channel length of 10 µm and channel width of 50 cm. The PANI film was produced using an oxidative polymerization process with phytic acid as the dopant.[30] The successful deposition of a homogeneous polymer film (thickness 150 nm) was confirmed by atomic force microscopy (Figure S1, Supporting Information). The transfer (drain current I_{DS} vs V_{GS}) and output (I_{DS} vs source–drain bias V_{DS}) characteristics presented in **Figure 2**A,B were obtained using the ionic liquid 1-butyl-3-methylimidazolium tetrafluoroborate as the electrolyte and a nonaqueous Ag/Ag^+ as the gate electrode.

The transfer characteristic sweeping from negative to positive V_{GS} in Figure 2A (solid line) shows a clear, symmetric peak in I_{DS} versus V_{GS}, with a maximum current of 2.43 ± 0.25 mA at V_{GS} = 0 V and V_{DS} = +0.1 V, corresponding to a channel conductivity of 32.3 ± 0.3 mS cm^{-1}. We divide this peak into two regions. The first region (blue) extends from –0.8 to 0 V, and is where *n*-like behavior is observed, i.e., more positive V_{GS} increases the conductivity. The second region (red) extends from 0 to +0.5 V, and is where *p*-like behavior is observed, i.e., more positive V_{GS} decreases the conductivity. We observe the same two regions as we sweep towards more negative V_{GS}, however with the peak current shifted by –100 mV. This hysteresis correlates with the hysteresis observed in the cyclic voltammetry (Figure S2, Supporting Information). Hysteresis has been reported for devices made of polythiophene, polypyrrole, and polyaniline, where the polymer has been highly oxidized

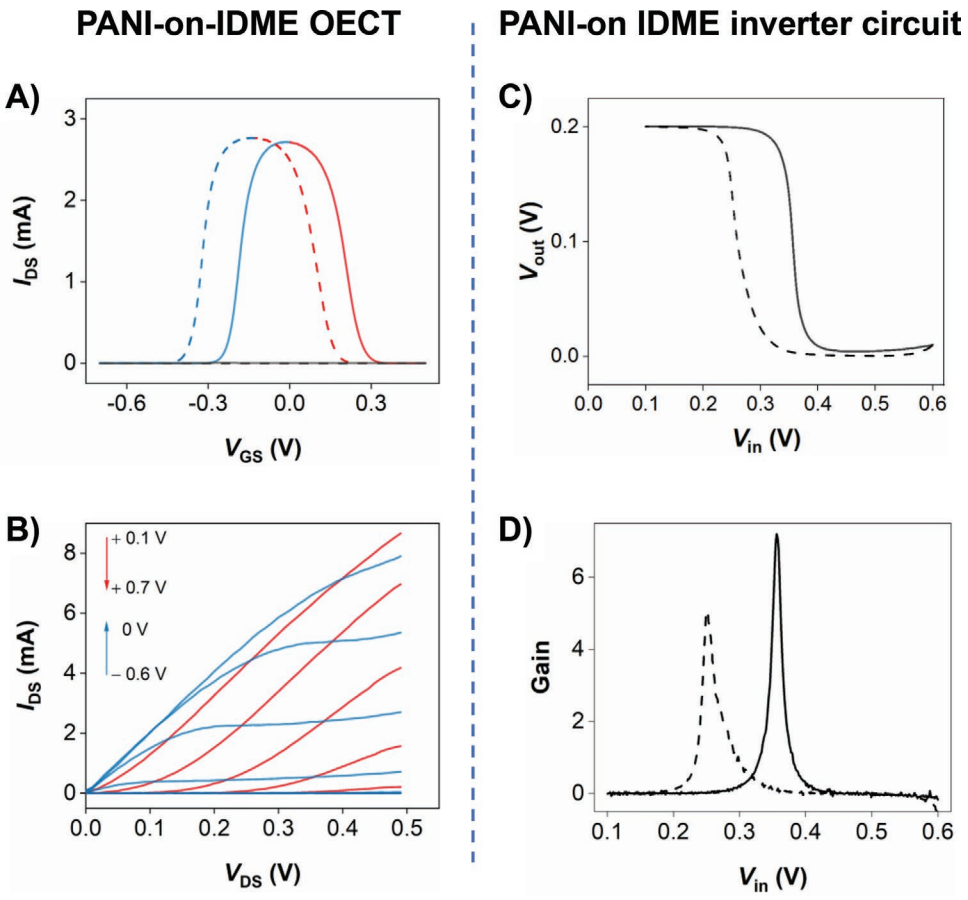

Figure 2. A) I_{DS} versus V_{GS} at V_{DS} = +0.1 V. Black lines represent the leakage current. B) I_{DS} versus V_{DS} for V_{GS} from –0.6 to 0 V (blue) and +0.1 to +0.7 V (red). Data on the *n*-slope and *p*-slope sides of the conductivity peak are presented in red/blue for both (A and B). C) Voltage-transfer characteristic (VTC) for our inverter circuit made using a pair of PANI-on-IDME OECTs connected by external wiring and operating with ionic liquid electrolyte. D) Corresponding voltage gain of the inverter. Positive and negative sweeps are presented by solid and dashed lines respectively.

© 2020 Wiley-VCH GmbH

without causing its degradation. The hysteresis was attributed to the transition between different oxidation states and the related changes in charge density of the polymer.[31–33] Other proposed mechanisms for the source of hysteresis include charge trapping due to defects in the semiconductor film or ion–polymer interactions hindering ion mobility.[34–37] The output characteristics in Figure 2B show behavior consistent with the transfer characteristics in Figure 2A. We repeated these measurements for our PANI-on-IDME OECT at V_{DS} = –0.1 V (Figure S3A,B, Supporting Information). Similarly, a current peak is observed as V_{GS} is increased toward positive potential.

2.2. Characterization of PANI-Based OECT Complementary Logic Circuits

We set out to investigate whether a single-material complementary circuit can be built using two identical OECTs, i.e., featuring the same active channel material PANI, based on the *n*-like and *p*-like behavior we have obtained from our PANI-based OECT. Figure 2C shows the voltage-transfer characteristic (VTC) for our inverter circuit (Figure 1B) with V_{DD} = +0.2 V and offset voltage V_{shift} = –0.4 V applied to the OECT closest to ground. We determined the value of V_{shift} from the transfer curves of the single OECTs used in the circuit, such that we obtain one OECT in its "on" state and the other in its "off" state (Figure S4, Supporting Information). There is a slight offset between the sweep from negative V_{in} to positive V_{in} (solid line) and sweep back from positive V_{in} to negative V_{in} (dashed line), consistent with the hysteresis previously shown in Figure 2A. Figure 2D shows the DC gain $\partial V_{out}/\partial V_{in}$ versus V_{in} with a peak gain of 7.2 obtained at the switching threshold V_M = +0.36 V. Our inverter gain is >1, meeting an essential functional criterion of an inverter.[10] It also has higher gain compared to the only conjugated polymer OECT-based complementary circuit reported to date (≈4) and measured at the same V_{DD}.[14] The ideal switching threshold for well optimized complementary inverter circuits is $V_{DD}/2$, and deviation of our inverter from this could arise for two key reasons. First, the switching thresholds are not symmetric about 0 V, i.e., $V_{Th,n} \neq -V_{Th,p}$, where $V_{Th,n}$ and $V_{Th,p}$ are the *n*-type and *p*-type switching thresholds (Figure S4C, Supporting Information), respectively. Second, the quantity $k = \mu C(Z/L)$, where μ is mobility, C is gate capacitance, Z is channel width and L is channel length, is not perfectly balanced for the two transistors,[10] as indicated by the different magnitude in saturation current exhibited by each device (Figure S4C, Supporting Information). The frequency response of the inverter to a square wave input is shown in Figure S5 (Supporting Information). The output voltage reflects the typical response of an inverter, although good signal fidelity can only be achieved at low frequency currently (≈0.1 Hz). Our PANI OECT-based complementary logic circuit can also function as an amplifier circuit when operated at negative V_{DD} = –0.2 V as shown in Figure S3C,D (Supporting Information). Although there is some room for improved performance through optimization, our work here represents the first proof-of-concept for an inverter circuit built from two OECTs featuring identical active channel material.

2.3. Simultaneous Transistor, Electrochemical and Optical Characterization of PANI-Based OECTs

PANI is a *p*-doped semiconductor in the presence of phytic acid. The origin of the transition between the *n*-like and *p*-like behavior we observe here is electrochemically driven. We show this by investigating the electrochemical and optical properties of PANI using custom-built apparatus (**Figure 3**A and Figure S6, Supporting Information) that enables simultaneous transistor, CV and UV–Vis measurements of a PANI-on-IDME structure as used in our OECT. The set-up is described in full detail in the Supporting Information. The intent here is to augment rather than replace properly engineered CV and UV–Vis instruments–we use the data obtained from this set-up to ensure that measurements taken using our CV and UV–Vis systems are correctly aligned in gate potential with the transistor characteristics.

Figure 3B presents measurements of I_{DS} (top), working electrode current I_{WE} (middle) and photodiode current (bottom) versus V_{GS}. The PANI clearly exhibits different characteristics defined by three distinct regions of potential: Region I (–0.8 to –0.1 V), Region II (–0.1 to +0.7 V), and Region III (+0.7 to +1.0 V). The cyclic voltammogram (middle) shows a typical redox process in which PANI changes oxidation states between leucoemeraldine (nonconductive and fully reduced–Region I), emeraldine (conductive–Region II) and pernigraniline (nonconductive and fully oxidized–Region III).[38,39] In Regions I and III, the Faradaic current is negligible, corresponding to the off states of the PANI OECT in the transfer characteristic. In contrast, the Faradaic current is significantly higher in Region II, indicating that the PANI is in the conductive form. The on state of the OECT coincides directly with Region II.

We concurrently measured the optical transmission via the photodiode current (Figure 3B bottom) since absorption spectroscopy enables the oxidation states of PANI (Figure 1C) to be identified.[39] Reduced photodiode current in Figure 3B corresponds to enhanced absorption. Only the 320 nm peak is observed when PANI is in its leucoemeraldine state. The emeraldine acid shows a peak at 430 nm accompanied by a broad shoulder centered at >800 nm. A blue shift of the polaron region to ≈650 nm or lower identifies the emeraldine base and pernigraniline states. Since the emeraldine acid is the most electrically conductive form of PANI, we chose to focus on the absorption at 428 nm (Figure 3B) and 850 nm (Figure S7, Supporting Information). In Figure 3B, the photodiode current remains constant and at maximal value for V_G < –0.22 V. We observed a sharp decrease in photodiode current at the boundary between Regions I and II. We attribute this sharp increase in absorption to protonation of the leucoemeraldine state to form the emeraldine acid state. We confirm this process with separate spectroelectrochemistry measurements shown in Figure 3C. As we move from Region I to Region II, we observe the weakening of the 320 nm peak corresponding to the leucoemeraldine state and strengthening of the 430 nm peak corresponding to the emeraldine acid state, indicating a transition between the two oxidation states. We observe fluctuations in the photodiode current with further increase in V_{GS} (Regions II and III; Figure 3B), but it remains low compared to its initial value at V_{GS} < –0.22 V. The fluctuations indicate further

© 2020 Wiley-VCH GmbH

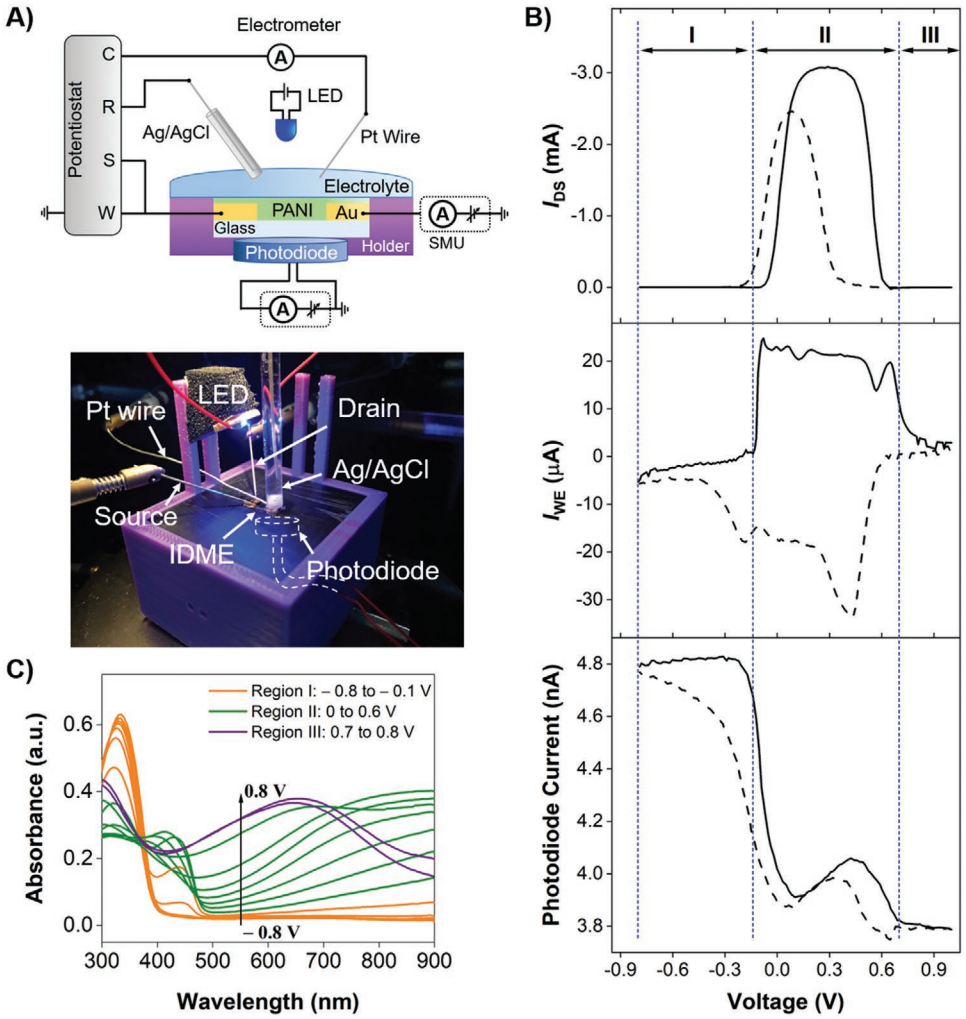

Figure 3. A) Schematic (top) and photograph (bottom) of the apparatus used for near-simultaneous measurements of transfer characteristics, cyclic voltammetry and UV–vis absorption. B) Plots of (top) I_{DS} at V_{DS} = −0.1 V, (middle) I_{WE} working electrode (WE) current and (bottom) photodiode current under 428 nm illumination versus V_{GS} swept at 50 mV s^{-1}. C) In situ spectroelectrochemistry of PANI film on ITO-coated glass as a function of applied potential between −0.8 and +0.8 V.

chemical change in the film; the emeraldine acid co-exists with the emeraldine base in Region II and converts to the pernigraniline state in Region III. The blue shift in the polaron region and decrease in 430 nm peak in Figure 3C further support this conclusion. We can identify with certainty that the nonconductive leucoemeraldine and pernigraniline states are the dominant species in Regions I and III respectively, where the OECT was in the off state, while the emeraldine state was dominant in Region II, where the OECT is in the on state by combining optical transmission and cyclic voltammetry measurements obtained while the OECT was operating.

2.4. Density Functional Theory Study of Conduction States in PANI OECTs

We performed density functional theory (DFT) calculations for PANI in different oxidation states to further understand Regions I–III. In previous studies,[40,41] analysis of the electronic states was performed for isolated PANI polymers, i.e., PANI surrounded by vacuum. Here, we explicitly simulate and analyze PANI in its different oxidation states while in contact with the Au electrode, an integral component in the OECT device. This is an original aspect of our simulations in comparison to the literature. To perform this type of simulation properly, we have carried out very intensive DFT+D calculations for a large system composed of 128 Au atoms, 52 organic ions, and a large vacuum region of 30 Å of length. We reveal, that in the absence of any defects, PANI was physisorbed on the gold substrate via hydrogen bonds of the Au···H-X type (Figure S8, Supporting Information).[42] The main interactions between the PANI polymer and the Au substrate are long-range dispersion-like with no considerable effect on the electronic band structure of the polymer.

We find that the leucoemeraldine base is strongly insulating owing to a wide band gap of 2.15 eV and a Fermi energy just above the valence band edge (Figure S9A, Supporting Information) in agreement with the experiments. For the emeraldine

© 2020 Wiley-VCH GmbH

acid state, we find empty electronic states at ≈0.1 eV above the valence band edge. These arise from polaron formation upon protonation of the leucoemeraldine polymer backbone. These empty states are sufficiently close to the valence band edge so that charge carriers can be excited upon application of a small electric bias making PANI an effective conductor (Figure S9B, Supporting Information). For the pernigraniline base, we find that the density of polaron states just above the valence band edge is increased as compared to the emeraldine state (Figure S9C, Supporting Information). Upon application of an appropriate electric field, it is possible to fill up such unoccupied electronic states and attain an insulator state characterized by an energy band gap of 1.55 eV. Overall, these calculations compare well with others in the literature,[40,41,43] and support the argument that the redox changes occurring in PANI lead to the conductance peak in the transfer characteristics.

2.5. Monolithic PANI-OECT Complementary Circuits on Flexible Biocompatible Substrates Operating in Aqueous Electrolyte

Low operating voltage is a vital property for building bioelectronic circuits, which inevitably need to operate in an aqueous electrolyte environment. An attractive aspect of PANI is that its electrochemical activity is within an ideal range for this purpose (<1 V) (Figure S2, Supporting Information). We have also previously shown that phytic-acid-doped PANI can be polymerized on a flexible biocompatible chitosan substrate to form an electronically and mechanically stable conductive patch, which we developed for electrically bridging infarcted cardiac tissue.[30] That put us in an ideal position to directly transfer our PANI OECT complementary circuits from non-monolithic glass IDMEs, i.e., separate glass IDME chips wired in an external circuit, to fully monolithic integrated on flexible biocompatible chitosan substrates [44–46] and actuated by aqueous electrolyte (**Figure 4**A). We show the transfer characteristics in Figure 4B for a single PANI-on-chitosan OECT obtained using 0.1 M NaCl aqueous electrolyte with an Ag/AgCl electrode as the reference electrode for supplying V_{GS}. The conductance peak is shifted to slightly lower V_{GS} (–0.08 V) compared to our devices on glass (Figure 2A). This shift may simply arise from differences in substrate charge between glass and chitosan. The peak current (0.63 mA) is lower for the same V_{DS}, which is more related to the change in transistor geometry than an intrinsic change in PANI properties.

Figure 4C,D shows VTC and corresponding gain for our PANI-on-chitosan inverter circuit (Figure 1C) with V_{DD} = +0.2 V and offset voltage V_{shift} = –0.4 V applied to the OECT closest to ground. We observe hysteresis similar to our PANI-on-IDME inverter and in agreement with the hysteresis recorded for the single PANI-on-chitosan OECT (Figure 4B). We obtain a peak gain of 2.4, lower than for our PANI-on-IDME circuit, which

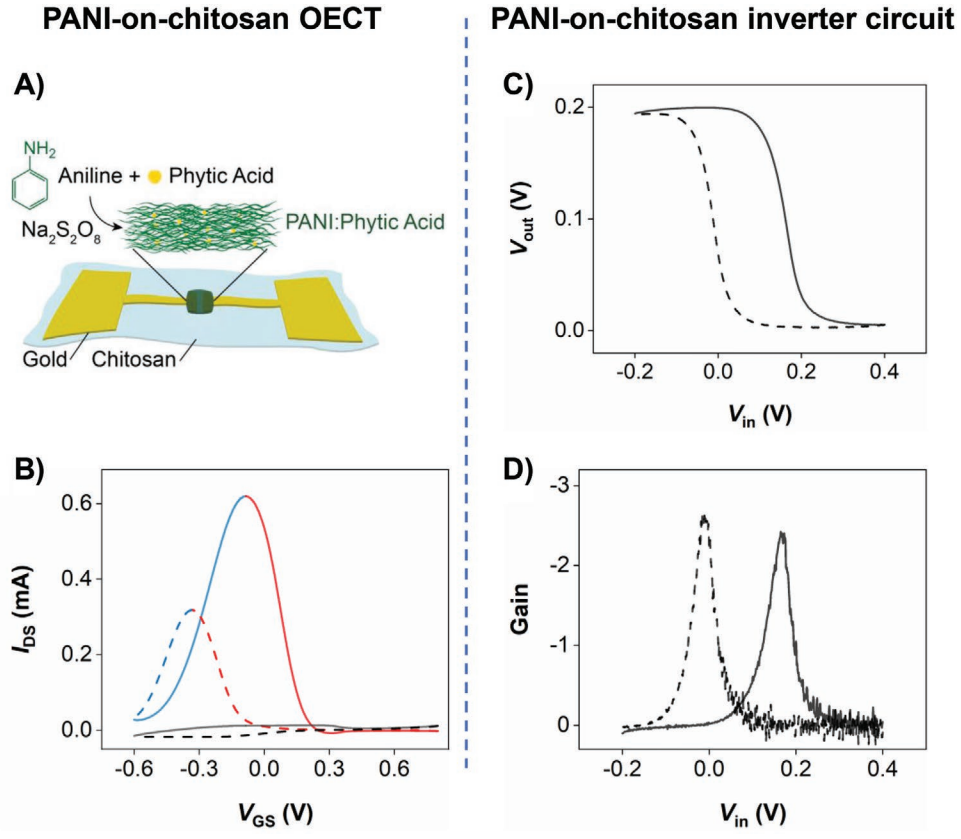

Figure 4. A) Schematic of the oxidative polymerization of PANI doped with phytic acid on a chitosan film with patterned Au electrodes on the surface. B) I_{DS} versus V_{GS} at V_{DS} = +0.1 V. Black lines represent the leakage current. C) VTC for inverter circuit made on flexible chitosan film operating with aqueous NaCl electrolyte. D) Corresponding voltage gain of the inverter. Positive and negative sweeps are presented by solid angd dashed lines respectively.

© 2020 Wiley-VCH GmbH

could arise either from a less optimal transistor geometry or trapping of electrolyte ions in the positively charged chitosan. We also evaluated the frequency response of the flexible PANI-on-chitosan inverter (Figure S10, Supporting Information). We achieved a response with a good signal fidelity at 0.1 Hz, similar to the PANI-on-IDME inverter. Transfer, output and VTC characteristics of the PANI-on-chitosan circuit operating at a negative $V_{DD} = -0.2$ V are shown in Figure S11 (Supporting Information).

3. Discussion and Conclusions

Introducing electronic circuits into bioelectronic devices will enable new and improved biomedical functionalities. Conjugated polymer based OECTs have demonstrated superior performance at the biointerface, in comparison to other transistor architectures such as the organic field-effect transistor (OFET) or the electrolyte-gated OFET.[47] This is due to the mixed electronic and ionic transport that OECT displays. OECTs have been largely explored as single devices despite the fact that transistors are rarely used alone and often built into integrated circuits for higher function. A few attempts have been recently made towards modifying or using the OECT as an elementary unit in building advanced electronic circuits,[47–50] with only one example reporting a conjugated polymer based complementary circuit.[14] We speculate that the lack of advancement in developing complementary circuits based on conjugated polymers is due to the limited choice of materials. Conjugated polymers are mostly *p*-type with very few *n*-type materials readily available.[16] Here, we overcome this limitation by taking a radical new approach toward building a complementary circuit driven by electrochemical processes. We demonstrate that a single material complementary circuit can be built from two identical PANI-based OECTs, eliminating the need for an *n*-type conjugated polymer. We achieve this by arranging the two identical OECTs in an inverter circuit and applying a small additional voltage to offset the operating point of one OECT relative to the other, thereby giving dc gain as high as 7.2. We transfer the technology on a chitosan substrate to build a flexible inverter with demonstrated functionality in aqueous electrolytes.

Further work is obviously required to optimize the performance of our device, which is a proof-of-concept with unique characteristics. We expect that the gain can be improved by enhancing the mobility of the device. This can be achieved by optimizing, e.g., the conjugation length, planar configuration, and chain packing of the PANI films.[51] The electrolyte and its solvent are also key factors to consider. The size and charge of an ion will dictate the speed of its diffusion in and out of the film, as well as its interaction with the active channel material. The type of solvent, whether it has a hydrating effect or non-wetting properties, will have an immediate impact on the morphology of the active channel and ion mobility.[52] Dedicated studies may be performed to probe whether the observed hysteresis can be minimized by controlling the charge density on the oxidized polymer (degree of doping), varying the processing conditions including the solvent and polymerization method, and investigating electrolytes of different size and charge. Our PANI-based OECT was fabricated by chemically polymerizing aniline on the electrode surface, accounting for slight variations in device geometry. The fabrication process can be improved by using photolithography or electropolymerization to enable control over the film thickness.[53] Minimizing variations in device geometry will be important to achieving equivalent saturation current between the two OECTs, and thereby shifting the inverter response closer to ideal behavior. These optimization measures should also have an immediate impact on improving the ac response of the devices.

Our work's key novelty is the application of the conductance peak in PANI OECT transfer characteristics to realize OECT-based complementary circuits using only a single common channel material. This was made possible because of the finite electrochemical window of PANI that is within a potential range suited for operation in water (<0.9 V). The conductance peak we observe in our PANI OECTs is consistent with literature,[22,24,32,54] and similar behavior has been shown for other conjugated polymers such as polypyrrole and polythiophenes, though for potentials >1 V.[31,55,56] The key point of novelty in our work is that this is the first time this electrochemically-driven conductance peak has been exploited for complementary circuit design to achieve a circuit featuring two OECTs with identical channel composition. Fan et al. proposed that a single material complementary circuit can be potentially built from two PEDOT-PSS OECTs, with one OECT in its pristine form (depletion mode) and the other in its over-oxidized form (accumulation mode).[48] A challenge in implementing this idea is that overoxidizing PEDOT results in a significant drop in current (order of 10^6) compared to the pristine PEDOT OECT.[48] In a complementary circuit configuration, using OECTs with mismatched transport properties limits circuit performance. There is thus a strong incentive to move to alternative materials such as PANI, as we have done here.

Our design approach to integrate the inverter circuit in the chitosan substrate enabled its operation in aqueous electrolyte, otherwise not possible due to the leaching of the dopant out of the active channel. We have previously shown that a conductive patch made from PANI-on-chitosan is electronically stable due to the immobilization of the dopant phytic acid in the patch through its strong chelation with chitosan.[30] We have also demonstrated that the patch electrocouples with damaged cardiac tissue increasing conduction velocity (≈25%), and is not proarrythmogenic following in vivo implantation.[30] This sets the foundation for the flexible complementary logic circuit we developed here for in vivo operation at the biointerface. The next step will be to optimize the response time of the circuit to process signals of physiological frequencies, toward its use as a real-time processing unit at the biointerface.[57] An alternative application to consider is memory and neuromorphic devices, which would exploit the hysteresis of our devices as a feature rather than a flaw.[6,58–61] The present work sheds a new light on conjugated polymers, extending their capabilities beyond use in a single OECT device but towards complementary logic circuits featuring OECTs with a common single channel material operating by electrochemical processes.

4. Experimental Section

Materials: All chemicals were purchased from Sigma Aldrich and used without any further purification. Any water used was deionized

© 2020 Wiley-VCH GmbH

to 18 MΩ.cm using a Millipore (Milli-DI) pro system unless otherwise specified.

PANI-on-IDME: OECTs were fabricated on interdigitated microelectrode (IDME) structures purchased from Micrux Technologies (ED-IDE1-Au). PANI films were obtained by oxidative polymerization of aniline directly on the IDME as described previously.[30,62] Briefly, solution 1 was prepared by mixing 470 µL phytic acid and 230 µL aniline in 1 mL of water. Solution 2 was prepared by dissolving 143 mg ammonium persulfate in 0.5 mL of water. Then, 7.7 µL of solution 1 and 2.3 µL of solution 2 were mixed in an Eppendorf tube and immediately transferred onto the IDME. The IDME was left for 3 h to allow for PANI polymerization. The reaction was quenched by rinsing with water until no PANI flaked off the surface.

PANI-on-Chitosan OECT: Chitosan substrates (20 µm thick) were prepared by dropcasting 1.6 mL of chitosan solution (1.5 wt% chitosan in 2 wt% acetic acid aqueous solution) on a microscope slide (76 mm × 25 mm).[63] Electrodes were deposited using a PVD75 vacuum thermal evaporator system with a shadow mask. The metallization was 5 nm Ti and 100 nm Au, with the Ti used to ensure good metal adhesion to the chitosan. The transistor channel had width 20 µm and length 2 mm. PANI was chemically polymerized in the conductive channel using the method previously described. This resulted in strong adhesion of PANI on the substrate due to the strong chelation between the negatively charged phytic acid and the positively charged PANI and chitosan.

Atomic Force Microscopy: IDME topography before and after PANI deposition was acquired using a JPK Instruments atomic force microscope with NanoWizard II software. The microscope was operated in contact mode in air using silicon cantilevers (AppNano ACT-50; Length 125 µm, width 30 µm, tip radius <10 nm) with 36 Nm^{-1} nominal spring constant and 200–400 kHz resonant frequency. Scanning rate was 1 Hz with pixel resolution 1024 × 1024.

In Situ UV–Vis Spectroelectrochemistry: PANI was polymerized on ITO slides (60 mm x 8 mm) to serve as the working electrode and put into a 3 mL cuvette containing 1-butyl-3-methylimidazolium tetrafluoroborate ionic liquid. A platinum wire and Ag/AgCl electrode in 0.1 M $AgNO_3$ (CHI Instruments) were immersed in the ionic liquid as counter and reference electrodes, with potential applied and current measured using an Ivium Vertex 100 mA potentiostat. The absorption spectra were obtained with a PerkinElmer Lambda 900 UV–Vis spectrometer over the 300 to 900 nm wavelength with 5 nm steps.

Electrical Characterization of the OECT: Transistor characteristics were measured using a pair of Keithley 2401 Source Measure Units (SMUs) and a Keithley 6517A electrometer. The first SMU supplied the drain–source voltage V_{DS} and measured source current I_{SD}, and the second SMU supplied the gate voltage V_{GS} and measured gate leakage current I_{GS} (via Ag/AgCl in 0.1 M $AgNO_3$ electrode; CHI Instruments). The electrometer measured the drain current I_{DS} flowing to virtual ground. Voltage sweeps were performed with a step of 1 mV. The electrical characteristics of the device on IDME and chitosan substrate were obtained using 1-butyl-3-methylimidazolium tetrafluoroborate ionic liquid and 0.1 M NaCl solution respectively. Conductivity of the channel (σ) was calculated using the following formula

$$\sigma = w/(R \cdot L \cdot t) \quad (1)$$

where R is the resistance, L and w are the length and width of the channel respectively, and t is the thickness of the PANI film.

Electrical Characterization of the OECT-Based Complementary Circuit: Two identical PANI-based OECTs were used to build the circuit. One device was operated as a *p*-like device and the other as an *n*-like device (refer to Figure S4 in the Supporting Information) by varying the input voltages at their gates. V_{in} was applied on the *p*-like device using a grounded Keithley 2401 source-measure unit (SMU). $V_{shift} + V_{in}$ was applied on *n*-like device using another Keithley 2401 SMU whose ground was V_{in} and its output set to $V_{shift} = -0.4$ V. The inverter supply voltage V_{DD} was also applied using a Keithley 2401 SMU. The output voltage V_{out} was acquired using a Keithley 2000 Multimeter. An Ag/AgCl in 0.1 M $AgNO_3$ electrode immersed in 1-butyl-3-methylimidazolium tetrafluoroborate was used for the logic circuit with PANI-on-IDME transistors and an Ag/AgCl in 0.1 M $AgNO_3$ electrode immersed in 0.1 M NaCl solution was used for the chitosan-based logic circuit.

Concurrent Measurements of Optical and Electrochemical properties: CV and UV–visible absorption spectroscopy (UV–Vis) are generally used to investigate the electrochemical and optical properties of PANI films. These are commonly performed on separate films/substrates under different experimental conditions using different instruments, making comparative analysis more challenging. To address this, an apparatus (shown in Figure 3A) was built that enabled transistor, CV, and UV–Vis measurements to be obtained from the PANI-on-IDME in exactly the form they were used in the OECT under identical conditions and nearly simultaneously. The apparatus consists of a box with a transparent upper window containing a 15 mm^2 Si photodiode (Centronic OSD15-5T) mounted directly underneath the 3.5 mm diameter active region of the glass IDME chip and used to measure transmitted light, which is proportional to induced photocurrent. The IDME was illuminated obliquely from above by an LED with wavelength 428 or 850 nm to accommodate the Ag/AgCl microelectrode contacting the ionic liquid electrolyte. The transistor and CV measurements were obtained with a hybrid set-up consisting of an Ivium Vertex potentiostat, a Keithley 6517A electrometer and a Keithley 2401 source-measure unit. For conventional CV measurements, the source and drain would be both connected to the working electrode, with the reference (Ag/AgCl) and counter (Pt) electrodes immersed in the ionic liquid sitting on the PANI transistor channel. The set-up in Figure 3A differs in two ways from this. First, only the drain electrode remains connected to the working electrode input for the potentiostat; the source electrode is instead connected to the Keithley 2401 to enable a source–drain bias V_{SD} to be applied. Second, a floating Keithley 6517A is put into the counter electrode line. This enabled us to measure the corresponding gate leakage current I_{GS} flowing via the counter electrode when a gate voltage V_{GS} is applied on the reference electrode. Note that this V_{GS} is identical to the voltage (V) applied in cyclic voltammetry, and the gate leakage current I_{GS} is equivalent to the current measured at the working electrode I_{WE} in a typical three electrode set-up. The cyclic voltammetry presented in Figure 3A was obtained by plotting I_{WE} versus V_{GS}. The potentiostat working electrode measures drain current I_{DS} and the Keithley 2401 enables to also measure source current I_{SD} while sourcing V_{DS}, giving full details for transistor characterization. For a pure CV trace, one would run $V_{DS} = 0$ V, with $I_{GS} = I_{SD} + I_{DS}$ giving the current I conventionally measured in this technique. It was confirmed that this combination of instruments did not adversely affect outcomes of either characterization, i.e., it gave transistor characteristics matching those obtained in the normal transistor characterization circuit and likewise for CV compared to the Ivium used alone.

Density Functional Theory Calculations: First-principles calculations based on density functional theory (DFT) [64] were done with the VASP code,[65] using the generalized gradient approximation to the exchange-correlation energy developed by Perdew et al.[66] Possible dispersion interactions in the system were captured with the D3 correction scheme developed by Grimme et al.[67] The projector-augmented-wave method was used to represent the ionic cores and the following electronic states were considered as valence: Au 5d–6s, C 2s–2p, O 2s–2p, and H 1s. Wave functions were represented in a plane-wave basis truncated at 750 eV and a force tolerance of 0.01 eV $Å^{-1}$ was imposed in the geometry optimizations. The energies of the optimized systems converged to within 2 meV per atom using the parameters above and a k-point grid of 1 × 2 × 2 for integration within the Brillouin zone. Large simulation boxes typically containing 180 atoms were employed to simulate the Au substrate/PANI systems (128 atoms for the gold substrate and 52 for the PANI). Periodic boundary conditions were applied along the three Cartesian directions and a vacuum region of ≈30 Å was considered in the simulation cell to avoid spurious interactions with the neighboring image systems (Figure S7, Supporting Information). It was checked that the simulation DFT results were appropriately converged with respect to the adopted PANI length of four carbon aromatic rings by carrying out additional calculations for longer polymers containing six monomer units.

© 2020 Wiley-VCH GmbH

Supporting Information

Supporting Information is available from the Wiley Online Library or from the author.

Acknowledgements

This work was funded by the Australian Research Council under DP170104024 and DP190102560. The work was performed in part using the NSW node of the Australian National Fabrication Facility and the Electron Microscope Unit within the Mark Wainwright Analytical Centre at UNSW Sydney. The authors would like to thank Dr. Giuseppe Tettamanzi for useful discussions. E.Z. thanks the Swedish Research Council (VR International Postdoc Grant #2017-06381) and the Royal Swedish Academy of Sciences (Kungl. Vetenskapsakademiens stiftelser, #LN2017-0035) for funding.

Conflict of Interest

The authors declare no conflict of interest.

Keywords

bioelectronic devices, complementary circuits, organic electrochemical transistors, polyaniline

Received: August 24, 2020
Published online:

[1] J. A. Rogers, *JAMA, J. Am. Med. Assoc.* **2015**, *313*, 561.
[2] D.-H. Kim, R. Ghaffari, N. Lu, J. A. Rogers, *Annu. Rev. Biomed. Eng.* **2012**, *14*, 113.
[3] T. Someya, Z. Bao, G. G. Malliaras, *Nature* **2016**, *540*, 379.
[4] D. T. Simon, E. O. Gabrielsson, K. Tybrandt, M. Berggren, *Chem. Rev.* **2016**, *116*, 13009.
[5] X. Strakosas, M. Bongo, R. M. Owens, *J. Appl. Polym. Sci.* **2015**, *132*, 41735.
[6] J. Rivnay, S. Inal, A. Salleo, R. M. Owens, M. Berggren, G. G. Malliaras, *Nat. Rev. Mater.* **2018**, *3*, 17086.
[7] D.-H. Kim, S. Richardson-Burns, L. Povlich, M. R. Abidian, S. Spanninga, J. L. Hendricks, D. C. Martin, in *Indwelling Neural Implants: Strategies for Contending with the In Vivo Environment* (Ed: W. M. Reichert), CRC Press/Taylor & Francis, Boca Raton, FL **2008**.
[8] S. H. Kim, K. Hong, W. Xie, K. H. Lee, S. Zhang, T. P. Lodge, C. D. Frisbie, *Adv. Mater.* **2013**, *25*, 1822.
[9] K. J. Baeg, D. Khim, D. Y. Kim, S. W. Jung, J. B. Koo, I. K. You, H. Yan, A. Facchetti, Y. Y. Noh, *J. Polym. Sci., Part B: Polym. Phys.* **2011**, *49*, 62.
[10] K. J. Baeg, M. Caironi, Y. Y. Noh, *Adv. Mater.* **2013**, *25*, 4210.
[11] E. J. Meijer, D. M. De Leeuw, S. Setayesh, E. Van Veenendaal, B. H. Huisman, P. W. M. Blom, J. C. Hummelen, U. Scherf, T. M. Klapwijk, *Nat. Mater.* **2003**, *2*, 678.
[12] R. J. Chesterfield, C. R. Newman, T. M. Pappenfus, P. C. Ewbank, M. H. Haukaas, K. R. Mann, L. L. Miller, C. D. Frisbie, *Adv. Mater.* **2003**, *15*, 1278.
[13] T. Takahashi, T. Takenobu, J. Takeya, Y. Iwasa, *Appl. Phys. Lett.* **2006**, *88*, 033505.
[14] H. Sun, M. Vagin, S. Wang, X. Crispin, R. Forchheimer, M. Berggren, S. Fabiano, *Adv. Mater.* **2018**, *30*, 1704916.
[15] A. Giovannitti, C. B. Nielsen, D. T. Sbircea, S. Inal, M. Donahue, M. R. Niazi, D. A. Hanifi, A. Amassian, G. G. Malliaras, J. Rivnay, I. McCulloch, *Nat. Commun.* **2016**, *7*, 13066.
[16] H. Sun, J. Gerasimov, M. Berggren, S. Fabiano, *J. Mater. Chem. C* **2018**, *6*, 11778.
[17] M. Bourgeaux, W. G. Skene, *Macromolecules* **2007**, *40*, 1792.
[18] J. T. Blaskovits, M. Leclerc, *Macromol. Rapid Commun.* **2019**, *40*, 1800512.
[19] D. Khodagholy, J. Rivnay, M. Sessolo, M. Gurfinkel, P. Leleux, L. H. Jimison, E. Stavrinidou, T. Herve, S. Sanaur, R. M. Owens, G. G. Malliaras, *Nat. Commun.* **2013**, *4*, 2133.
[20] S. Z. Bisri, S. Shimizu, M. Nakano, Y. Iwasa, *Adv. Mater.* **2017**, *29*, 1607054.
[21] E. Stavrinidou, R. Gabrielsson, E. Gomez, X. Crispin, O. Nilsson, D. T. Simon, M. Berggren, *Sci. Adv.* **2015**, *1*, e1501136.
[22] E. W. Paul, A. J. Ricco, M. S. Wrighton, *J. Phys. Chem.* **1985**, *89*, 1441.
[23] J. C. Chiang, A. G. MacDiarmid, *Synth. Met.* **1986**, *13*, 193.
[24] S. Chao, M. S. Wrightor, *J. Am. Chem. Soc.* **1987**, *109*, 6627.
[25] A. Sliow, Z. Ma, G. Gargiulo, D. Mahns, D. Mawad, P. Breen, M. Stoodley, J. Houang, R. Kuchel, G. C. Tettamanzi, R. D. Tilley, S. J. Frost, J. Morley, L. Longo, A. Lauto, *Adv. Sci.* **2019**, *6*, 1801212.
[26] H. Ruprai, S. Romanazzo, J. Ireland, K. Kilian, D. Mawad, L. George, R. Wuhrer, J. Houang, D. Ta, S. Myers, A. Lauto, *ACS Appl. Mater. Interfaces* **2019**, *11*, 32613.
[27] D. Mawad, C. Warren, M. Barton, D. Mahns, J. Morley, B. T. T. Pham, N. T. H. Pham, S. Kueh, A. Lauto, *Carbohydr. Polym.* **2015**, *121*, 56.
[28] M. J. Barton, J. W. Morley, M. A. Stoodley, S. Shaikh, D. A. Mahns, A. Lauto, *J. Biophotonics* **2015**, *8*, 196.
[29] M. Barton, J. W. Morley, M. A. Stoodley, K.-S. Ng, S. C. Piller, H. Duong, D. Mawad, D. A. Mahns, A. Lauto, *J. Biophotonics* **2013**, *6*, 938.
[30] D. Mawad, C. Mansfield, A. Lauto, F. Perbellini, G. W. Nelson, J. Tonkin, S. O. Bello, D. J. Carrad, A. P. Micolich, M. M. Mahat, J. Furman, D. Payne, A. R. Lyon, J. J. Gooding, S. E. Harding, C. M. Terracciano, M. M. Stevens, *Sci. Adv.* **2016**, *2*, e1601007.
[31] D. Ofer, L. Y. Park, R. R. Schrock, M. S. Wrighton, *Chem. Mater.* **1991**, *3*, 573.
[32] C. H. McCoy, M. S. Wrighton, *Chem. Mater.* **1993**, *5*, 914.
[33] S. Y. Lee, G. R. Choi, H. Lim, K. M. Lee, S. K. Lee, *Appl. Phys. Lett.* **2009**, *95*, 23.
[34] A. Salleo, R. A. Street, *Phys. Rev. B: Condens. Matter Mater. Phys.* **2004**, *70*, 235324.
[35] H. L. Cheng, W. Q. Lin, F. C. Wu, *Appl. Phys. Lett.* **2009**, *94*, 3.
[36] E. Lim, B. J. Jung, M. Chikamatsu, R. Azumi, Y. Yoshida, K. Yase, L. M. Do, H. K. Shim, *J. Mater. Chem.* **2007**, *17*, 1416.
[37] G. Paasch, S. Scheinert, A. Herasimovich, I. Hörselmann, T. Lindner, *Phys. Status Solidi Appl. Mater. Sci.* **2008**, *205*, 534.
[38] Y. Wang, K. Levon, *Macromol. Symp.* **2012**, *317–318*, 240.
[39] J. E. Yoo, Y.-L. Loo, T. J. Dennes, J. Tarver, J. Schwartz, *Chem. Mater.* **2008**, *21*, 280.
[40] A. Varela-Álvarez, J. A. Sordo, G. E. Scuseria, *J. Am. Chem. Soc.* **2005**, *127*, 11318.
[41] X. P. Chen, J. K. Jiang, Q. H. Liang, N. Yang, H. Y. Ye, M. Cai, L. Shen, D. G. Yang, T. L. Ren, *Sci. Rep.* **2015**, *5*, 16907.
[42] H. Schmidbaur, H. G. Raubenheimer, L. Dobrzańska, *Chem. Soc. Rev.* **2014**, *43*, 345.
[43] K. M. Molapo, P. M. Ndangili, R. F. Ajayi, G. Mbambisa, S. M. Mailu, N. Njomo, M. Masikini, P. Baker, E. I. Iwuoha, *Int. J. Electrochem. Sci.* **2012**, *7*, 11859.
[44] C. Cui, N. Faraji, A. Lauto, L. Travaglini, J. Tonkin, D. Mahns, E. Humphrey, C. Terracciano, J. J. Gooding, J. Seidel, D. Mawad, *Biomater. Sci.* **2018**, *6*, 493.
[45] A. Lauto, M. Stoodley, M. Barton, J. W. Morley, D. A. Mahns, L. Longo, D. Mawad, *J. Visualized Exp.* **2012**, *68*, e4158.
[46] S. J. Frost, D. Mawad, M. J. Higgins, H. Ruprai, R. Kuchel, R. D. Tilley, S. Myers, J. M. Hook, A. Lauto, *NPG Asia Mater.* **2016**, *8*, e280.

© 2020 Wiley-VCH GmbH

[47] G. D. Spyropoulos, J. N. Gelinas, D. Khodagholy, *Sci. Adv.* **2019**, *5*, eaau7378.
[48] J. Fan, S. S. Rezaie, M. Facchini-Rakovich, D. Gudi, C. Montemagno, M. Gupta, *Org. Electron.* **2019**, *66*, 148.
[49] S. Fabiano, N. Sani, J. Kawahara, L. Kergoat, J. Nissa, I. Engquist, X. Crispin, M. Berggren, *Sci. Adv.2017*, 3, e1700345.
[50] W. Lee, D. Kim, N. Matsuhisa, M. Nagase, M. Sekino, G. G. Malliaras, T. Yokota, T. Someya, *Proc. Natl. Acad. Sci. USA* **2017**, *114*, 10554.
[51] R. J. Kline, M. D. McGehee, *Polym. Rev.* **2006**, *46*, 27.
[52] S. Inal, G. G. Malliaras, J. Rivnay, *Nat. Commun.* **2017**, *8*, 1767.
[53] A. Guiseppi-Elie, S. R. Pradhan, A. M. Wilson, D. L. Allara, P. Zhang, R. W. Collins, Y. T. Kim, *Chem. Mater.* **1993**, *5*, 1474.
[54] D. Ofer, R. M. Crooks, M. S. Wrighton, *J. Am. Chem. Soc.* **1990**, *112*, 7869.
[55] H. S. White, G. P. Kittlesen, M. S. Wrighton, *J. Am. Chem. Soc.* **1984**, *106*, 5375.
[56] J. W. Thackeray, H. S. White, M. S. Wrighton, *J. Phys. Chem.* **1985**, *89*, 5133.
[57] C. Cea, G. D. Spyropoulos, P. Jastrzebska-Perfect, J. J. Ferrero, J. N. Gelinas, D. Khodagholy, *Nat. Mater.* **2020**, *19*, 679.
[58] B. Winther-Jensen, B. Kolodziejczyk, O. Winther-Jensen, *APL Mater.* **2015**, *3*, 014903.
[59] G. Tarabella, P. D'Angelo, A. Cifarelli, A. Dimonte, A. Romeo, T. Berzina, V. Erokhin, S. Iannotta, *Chem. Sci.* **2015**, *6*, 2859.
[60] A. V. Emelyanov, D. A. Lapkin, V. A. Demin, V. V. Erokhin, S. Battistoni, G. Baldi, A. Dimonte, A. N. Korovin, S. Iannotta, P. K. Kashkarov, M. V. Kovalchuk, *AIP Adv.* **2016**, 6, 111301.
[61] Y. Van De Burgt, A. Melianas, S. T. Keene, G. Malliaras, A. Salleo, *Nat. Electron.* **2018**, *1*, 386.
[62] A. P. Hoang, H. Ruprai, K. Fidanovski, M. Eslami, A. Lauto, J. Daniels, D. Mawad, *Appl. Mater. Today* **2019**, *15*, 315.
[63] C. Cui, N. Faraji, A. Lauto, L. Travaglini, J. Tonkin, D. Mahns, E. Humphrey, C. Terracciano, J. J. Gooding, J. Seidel, D. Mawad, *Biomater. Sci.* **2018**, *6*, 493.
[64] C. Cazorla, J. Boronat, *Rev. Mod. Phys.* **2017**, *89*, 035003.
[65] G. Kresse, J. Furthmüller, Y. J. Li, Y. J. Chen, J. C. Walmsley, R. H. Mathinsen, S. Dumoulin, H. J. Roven, S. Yip, T. Supervisor, S. Chen, *Phys. Rev. B* **2000**, *62*, 8295.
[66] J. P. Perdew, K. Burke, M. Ernzerhof, *Phys. Rev. Lett.* **1996**, *77*, 3865.
[67] S. Grimme, J. Antony, S. Ehrlich, H. Krieg, *J. Chem. Phys.* **2010**, *132*, 154104.

© 2020 Wiley-VCH GmbH